Analytical Inverse Kinematics and Self-Motion Application for 7-DOF Redundant Manipulator

MINGDE GONG[1], XIANGDONG LI[2], AND LEI ZHANG[ID][3]
[1]School of Mechanical Engineering, Yanshan University, Qinhuangdao 066004, China
[2]SINOMACH Intelligence Technology Co., Ltd., Guangzhou, China
[3]School of Mechanical Science and Engineering, Jilin University, Changchun 130022, China

Corresponding author: Xiangdong Li (oridong@126.com)

ABSTRACT This paper studies multiple inverse kinematics solutions for a 7-DOF human redundant manipulator with a special joint configuration. A method is proposed for determining the continuous joint angle vector by selecting the inverse solution from discrete multiple solutions to the continuous end path of the mechanical arm. The elbow angle constraint is introduced, and the mapping relationship from the elbow angle to the joint angle is established. Subspaces are found in the multiple solution spaces to avoid joints exceeding the limit to obtain elbow angle interval, and then combined with the collision detection technique, subspaces are sought in multiple solution spaces to avoid collisions between robotic arms and obstacles. Two subspaces are then obtained, and with use of their intersection, all feasible manipulator inverse kinematic solutions that avoid the joint limit and the obstacles at a given pose are obtained. The above method explicitly determines the complete feasible kinematic inverse solution of redundant manipulators. Finally, the validity of the methods is verified via kinematic simulations.

INDEX TERMS Redundant manipulator, inverse kinematics, self-motion, joint limit avoidance, obstacle avoidance.

I. INTRODUCTION

7-DOF redundant manipulators have high flexibility owing to their self-motion characteristics. Several methods have been previously applied to inverse kinematic solutions [1]–[8]. For example, Zhou *et al.* [1] proposed a position-based approach to evaluating ranges of feasible inverse kinematic solutions and searching for the optimal solution, which is estimated on the basis of the disturbance acting on the base of the manipulator to obtain the optimal solution. Sciavicco and Siciliano [2] presented an algorithm that is based on a dynamic reformulation of the problem, leading to a closed-loop scheme; the stability of the latter is guaranteed by the selection of control that involves only the computation of the direct kinematics of the manipulator. Liu *et al.* [3] introduced key positions defined as Cartesian positions of the manipulator's elbow and wrist joints. The key positions are used as constraints on the inverse kinematics in addition to orientation constraints at the end-effector, such that the inverse kinematics can be calculated through an efficient

analytical scheme and realizes human-like configurations. Studies of the avoidance of joint limit or obstacle avoidance through self-motion characteristics are the research hotspot of redundant freedom manipulators [9]–[14].

Several approaches addressing the problem of avoidance joints are based on the joint velocity vector of the Jacobian matrix null space. These methods construct an exclusion factor using the joint limit value or build an attractor using the average of the joint limit to restrain the joint rotation angle. These techniques' can obtain a feasible solution but cannot fully utilize the complete range of the avoidance joints [15]–[18].

For the problem of the arm avoiding obstacles, most methods choose key points on the robotic arm, then construct a potential field to reject the manipulator arm position by using the distance of the key point to the obstacle [19]–[22]. These methods' biggest disadvantage is that falling into local extrema is easy in complex situations. These results have solutions but cannot be solved. Selecting the key points is challenging in the process of robot arm movement; for joint limit constraint avoidance and obstacle avoidance, several approaches introduce neural network algorithms to solve the

---

The associate editor coordinating the review of this manuscript and approving it for publication was Zeyang Xia.

model on the basis of an artificial potential field [23]–[25]. This approach is too complicated, and explicitly applying the self-motion characteristic method is effective and intuitive in obtaining a completely feasible solution.

The dynamic models of redundant freedom robotic manipulators are discussed for path planning [26]–[27]. The procedures required to derive the relevant motion equations become more laborious and complicated. To overcome this difficulty, it is essential to apply a recursive formulation to automatically obtain the governing equations. There are numerous recursive algorithms that can be applied to open kinematic chain systems [28]. In fact, by imposing the additional kinematic constraints, the extra DOFs were used to accomplish the other purposes, not to maximize the allowable load. Korayem *et al.* [29], [30] showed that, for a mobile base manipulator, there exists a position in which the manipulator can carry the maximum payload along a given path. Thus, the additional DOFs were used to place the base in the optimum location.

At present, the 7-DOF redundant manipulator trajectory planning method is equivalent to direct sampling of a seven-dimensional configuration space. To further determine whether the joint angles satisfy the obstacle condition and the joint motion range, repeated solutions and multiple judgments are necessary before the crawling task can be completed. Moreover, trajectory planning efficiency is low.

This research chooses the elbow angle as the supplementary control parameter, establishes the mapping relationship between the elbow angle and the working space and then divides the working space into the joint and obstacle avoidance spaces. Then, the intersection of the two subspaces is determined to obtain the inverse solution of motion satisfying the limit of avoiding joints and avoiding obstacles. The proposed method not only can obtain the joint angle that satisfies the trajectory planning but also render the inverse solution of the redundant manipulator an explicit solution. This outcome significantly improves trajectory planning efficiency and provides an effective method of further optimizing the independent control of redundant-DOF manipulators.

II. ANALYSIS OF THE INVERSE KINEMATIC SOLUTION

A. 7-DOF MANIPULATOR MODEL

We use the KUKA LBR iiwa robot as the model; the D-H parameters are shown in Table 1.

According to the standard D-H method adopted by MATLAB Robotic Tools, the coordinate system is shown in Figure 1.

B. SELF-MOTION PARAMETER MODEL

The origin of the first frame is moved to the origin of the second frame, thereby coinciding the robot's first three joint coordinates as shown in Figure 2.

First, θ_1 is rotated around the Z1 axis; then, θ_2 is rotated around the Z2 axis; then, θ_3 is rotated around the Z3 axis. This process is equivalent to rotating θ_1 around the Z1 axis

TABLE 1. KUKA LBR iiwa 14 R820 robot D-H parameters.

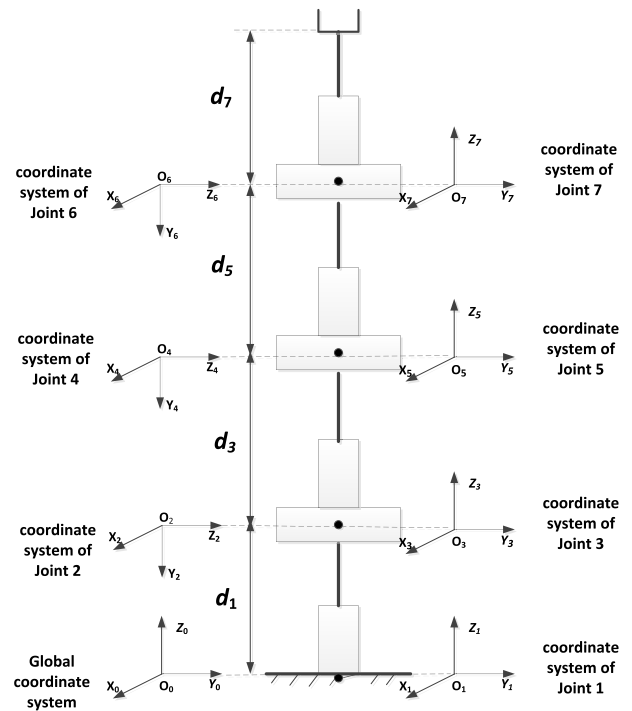| i	$^{i-1}T_i$	Joint parameters			Link parameters	
		θ_i (°)	$[\theta_i^l \quad \theta_i^u]$ (°)	d_i (m)	α_i (°)	a_i (m)
1	$^0T_1$	θ_1	[-170 170]	0.360	-90	0
2	$^1T_2$	θ_2	[-120 120]	0	90	0
3	$^2T_3$	θ_3	[-170 170]	0.420	-90	0
4	$^3T_4$	θ_4	[-120 120]	0	90	0
5	$^4T_5$	θ_5	[-170 170]	0.400	-90	0
6	$^5T_6$	θ_6	[-120 120]	0	90	0
7	$^6T_7$	θ_7	[-175 175]	0.126	0	0

FIGURE 1. Configuration and joint coordinate system of the robot.

first, then rotating around the rotated Y1 axis by θ_2 and finally rotating around the rotated Z1 axis by θ_3. The rotation of the first three joints is equivalent to a spherical joint with the center of the two coordinates' origin. Similarly, the rotation of the last three joints is also equivalent to that of a spherical joint, and the robot is equivalent to a human arm. The first three joints are equivalent to the shoulder joints S, the fourth joint is equivalent to the elbow joint E, the last three joints are equivalent to the wrist joints W and the end effector is equivalent to the palm T. When the end pose is given,
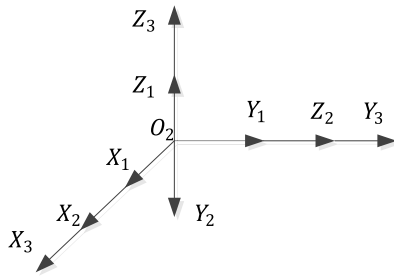
FIGURE 2. Top three joint coordinates of the same point.

the rotation of the last joint has no effect on the position of the end, the position of the wrist joint is fixed and the rotation of the first joint does not change the position of the shoulder joint. Therefore, when the end pose is fixed, the elbow joint rotates around the axis where the shoulder and wrist joint are connected, as shown in Figure 3.
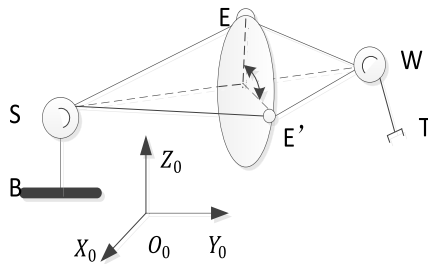

FIGURE 3. Elbow joint trajectory of the self-motion.

In this work, self-motion, that is, the circular motion of the elbow joint is called a redundant circle. We regard the vertical upward radius at the highest point on the circle as the starting axis, and the elbow joint is located on the radius of the angle Ψ at a certain moment. If the joint's angle limit is not considered, then the range of Ψ is $[-\pi, \pi]$. This feature introduces another constraint to the robot's movement pose, which is called the elbow angle. The six constraints of the end pose and the elbow angle constitute seven constraints, and the seven angles can be obtained using the geometric method. The elbow angle directly reflects the elbow's position in space, and the elbow angle is set to avoid the joint limit and the obstacle.

C. KINEMATIC ANALYSIS
Given that the elbow angle directly reflects the position of the elbow joint in space, the six constraints with the end pose to form a total of seven constraints, which is equivalent to introducing another constraint to the manipulator's motion pose. Accordingly, the geometrical method can be used to obtain the joint angle of 7 DOF.

The mapping relationship between the elbow angle and the joint angle of the manipulator is established, and the geometrical method is adopted to solve the arm angle range satisfying the limit of the seven joint corners. Then, the hollow spindle

formed by the movement of the robot arm intersects with the obstacle, obtaining the arm angle interval that avoids obstacles. Using the intersection of this interval and the arm angle interval of the joint avoidance limit, all feasible inverse solutions to avoid joint limits and obstacles in a given end-effector pose are obtained, thus acquiring complete values for subsequent dynamic optimization. The elbow arm angle is used as the constraint control parameter, which not only explicitly utilizes the advantages of the self-motion characteristic of the redundant DOF in the trajectory planning, but also conforms to the actual situation in which a person usually adjusts the elbow position to complete the grasping action.
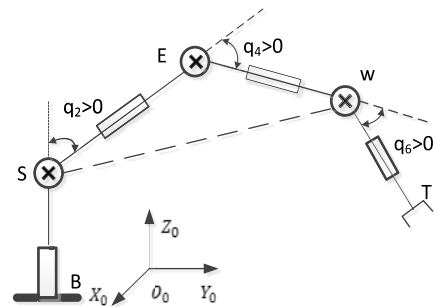

FIGURE 4. General position of the robot.

The general position of the robot is shown in Figure 4, in which $\otimes$ indicates that the vertical paper facing inward is positive and $\odot$ indicates that the vertical paper facing outward is negative (the same as below). d_{BS} is the distance between points B and S, d_{SE} is the distance between points S and E, d_{EW} is the distance between points E and W and d_{WT} is the *distance between points W and T. From the D-H table,* $d_{BS} = d1, d_{SE} = d3, d_{EW} = d5$ and $d_{WT} = d7$ are known. The S position is p_S.
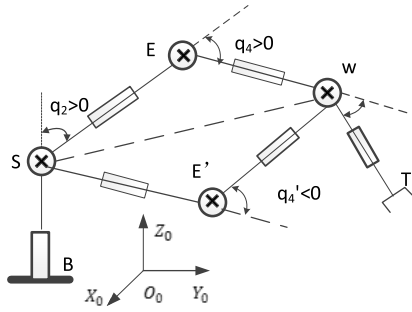
$$p_S = [0, 0, d_{BS}]^T \tag{1}$$

Given the end pose T_d, the position of point W is obtained by moving the end position d_{WT} in the opposite direction of Z7. The W position is p_W; then,

$$\begin{bmatrix} p_W \\ 1 \end{bmatrix} = T_d * \begin{bmatrix} 0 \\ 0 \\ -d_{WT} \\ 1 \end{bmatrix}. \tag{2}$$

In self-motion, three points SEW form a triangle, and the side length of the triangle is fixed. Using the vector $v_{SW} = p_W - p_S$, the module length is taken $d_{SW} = \|v_{SW}\|$. If $d_{SW} \geq d_{SE} + d_{EW}$, then the given pose is at the working space limit, which should be avoided. This finding also shows that SEW can form a triangle when the end position is within the workspace. Using the cosine theorem, we can obtain

$$\cos \angle SEW = \frac{d_{SE}^2 + d_{EW}^2 - d_{SW}^2}{2 \times d_{SE} \times d_{EW}}. \tag{3}$$

After a given T_d, $\angle SEW$ has a positive and negative solution satisfying Equation (6), as shown in Figure 5.

FIGURE 5. Two types of solutions of joint 4.

FIGURE 6. Plane defined by the three points SEW of the robot and coordinates Σ_{arm}.

In the figure, SEWE' forms a parallelogram, causing the elbow to be in a position above and below the line SW. Both positions are feasible for the end pose. Variable elbow is introduced as

$$\text{elbow} = \begin{cases} +1, & \text{elbow on the top} \\ -1, & \text{elbow on the below} \end{cases}. \quad (4)$$

Elbow reflects the position of the elbow joint relative to SW when the elbow angle $\Psi = 0$. The angle of joint 4 can be calculated as

$$q_4 = elbow \times (pi - acos(cos\angle SEW)). \quad (5)$$

The rotation angle of joint 4 is constant in the self-motion space and related only to the given end pose.

Owing to the circular motion of the elbow joint position, the plane $plSEW$, consisting of points S, E and W, rotates around the SW connection. Joint 5 does not change the position of W; joint 4 has a constant rotation angle; the posture of plane $plSEW$ is affected only by joints 1, 2 and 3. The three points on the plane are utilized to generate a coordinate system Σ_{arm} (abbreviation Σ) having an origin at S; the X^Σ axis direction is taken from S point to W, with Y^Σ perpendicular to the plane, as shown in Figure 6. Then, we can obtain

$$\begin{cases} X^\Sigma = \dfrac{v_{SW}}{\|v_{SW}\|} \\ Y^\Sigma = \dfrac{Z_0 \times X^\Sigma}{\|Z_0 \times X^\Sigma\|} \\ Z^\Sigma = X^\Sigma \times Y^\Sigma. \end{cases} \quad (6)$$
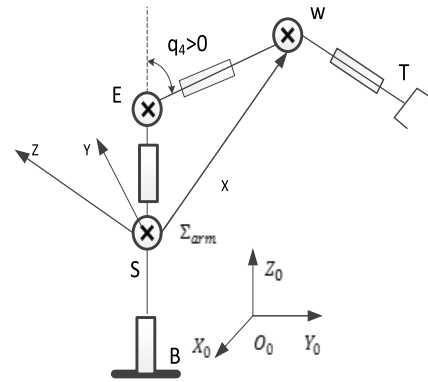
When the three current joint angles are all 0, Σ_{arm} is Σ_{arm_o} (abbreviated as Σ_o).

$$\mathbf{p}_W = \begin{bmatrix} d_{EW} * \sin q_4 \\ 0 \\ d_{BS} + d_{SE} + d_{EW} * \cos q_4 \end{bmatrix} \quad (7)$$

$$v_{SW} = \mathbf{p}_W - \mathbf{p}_S \quad (8)$$

Then, $\mathbf{Z}_0 = [0, 0, 1]^T$ is used, and Equations (7) and (8) are placed in Equation (6) to determine $X^{\Sigma_o}, Y^{\Sigma_o}, Z^{\Sigma_o}$; we can then obtain

$$\Sigma_o = \begin{bmatrix} X^{\Sigma_o} & Y^{\Sigma_o} & Z^{\Sigma_o} \end{bmatrix} \quad (9)$$

When the three current joint rotation angles turn to q_1, q_2, q_3, the coordinate system Σ_{arm} is Σ_D. For Σ_D, the coordinate system $\Sigma_D^{\Psi=0}$ is firstly determined when the elbow angle $\Psi = 0$. Equations (1) and (2) are placed in Equation (6) to determine $\Sigma_D^{\Psi=0}$, $\Sigma_D^{\Psi=0}$ around its own X-axis rotation angle Ψ. Then, Equation (10) is used to determine Σ_D.

$$\Sigma_D = \Sigma_D^{\Psi=0} \times Rot(x, \Psi) \quad (10)$$

In summary, given the end pose T_d and the elbow angle Ψ, $\Sigma_o, \Sigma_D^{\Psi=0}, \Sigma_D$ can be found.

If the shoulder S-spheroidal transformation formula is R_S, then $R_S \times \Sigma_o = \Sigma_D$; given that Σ_o, Σ_D form an orthogonal matrix, the following constantly exist:

$$\mathbf{R}_S = \Sigma_D \times \Sigma_o^T = \Sigma_D^{\Psi=0} \times Rot(x, \Psi) \times \Sigma_o^T. \quad (11)$$

By contrast, the spherical hinge transformation formula is

$$\mathbf{R}_s(q_1, q_2, q_3) = [Rot(Z, q_1)] \times [Rot(Y, q_2)] \times [Rot(Z, q_3)]. \quad (12)$$

That is,

$$\mathbf{R}_s(q_1, q_2, q_3) = \begin{bmatrix} * & * & C_1 S_2 \\ * & * & S_1 S_2 \\ -C_3 S_2 & S_2 S_3 & C_2 \end{bmatrix}. \quad (13)$$

In Formula (13), S_i, C_i mean $\sin(q_i), \cos(q_i)$; separately, $i = 1, 2, 3$. $*$ indicates that this item is ignored.

Then, $\cos(q_2) = R_s(3, 3)$; the q_2 determined from the formula has two values (positive and negative), as shown in Figure 7.

For the same elbow joint position, a set of q $= [q_1, q_2]^T$ solutions and another set of solutions $q = [q_1 + pi, -q_2]^T$ exist. Both solution sets are satisfied under this condition. The Y_1 pointer indicates whether the big arm is to the right or left of the $X_0 Z_0$ plane. The variable arm is introduced to reflect this location.

$$\text{arm} = \begin{cases} +1, & \text{arm on the right} \\ -1, & \text{arm on the left} \end{cases} \quad (14)$$
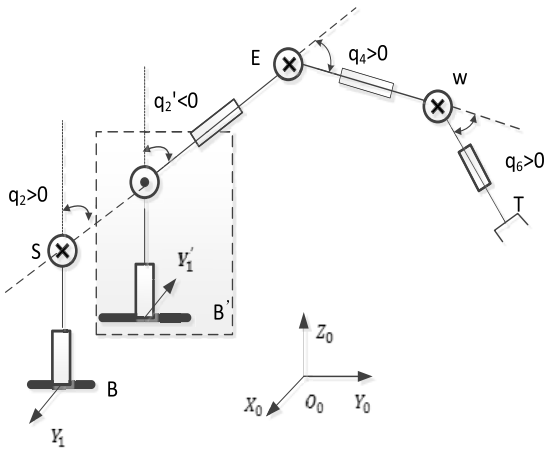
FIGURE 7. Multiplicity of solutions arising from joint q2.

Then,

$$q_2 = arm * acos\,(Rs(3, 3)] \tag{15}$$

When arm is 1, $\sin(q_2) > 0$; when arm is -1, $\sin(q_2) < 0$. According to Formula (13),

$$q_1 = atan2(arm*R_s(2, 3),\quad arm*R_s(1, 3)) \tag{16}$$
$$q_3 = atan2(arm*R_s(3, 2),\quad -1*arm*R_s(3, 1)). \tag{17}$$

When $\boldsymbol{T}_d$ is expressed as $\boldsymbol{T}_d = \begin{bmatrix} {}^0R_7 & {}^0p_7 \\ 0 & 1 \end{bmatrix}$, the end ges-
ture ${}^0R_7$ can be determined. The last three joints are defined as the wrist, and the transformation is represented by R_w. Then, Formula (18) is established.

$$\boldsymbol{R}_s \times Rot\,(y, q_4) \times \boldsymbol{R}_w = {}^0\boldsymbol{R}_7 \tag{18}$$

Given that the $\boldsymbol{R}_s \times Rot\,(y, q_4)$ result is an orthogonal matrix,

$$\boldsymbol{R}_w = {}^0\boldsymbol{R}_7 \times (\boldsymbol{R}_s \times Rot\,(y, q_4))^{\mathrm{T}} \tag{19}$$

Similarly,

$$\boldsymbol{R}_w\,(q_5, q_6, q_7) = \begin{bmatrix} * & * & C_5S_6 \\ * & * & S_5S_6 \\ -C_7S_6 & S_6S_7 & C_6 \end{bmatrix} \tag{20}$$

In this formula, S_i, C_i mean $\sin(q_i)$, $\cos(q_i)$; separately, $i = 5, 6, 7$.

$\cos(q_6) = R_w(3, 3)$; similarly, q_6 has two sets of solutions. The previous practice is followed, and the variable wrist is introduced as

$$wrist = \begin{cases} +1, & \text{wrist without flip} \\ -1, & \text{wrist with flip;} \end{cases} \tag{21}$$

then,

$$q_6 = wrist * acos(R_w(3, 3)) \tag{22}$$

When wrist is 1, $\sin(q_6) > 0$; when wrist is -1, $\sin(q_6) < 0$.
From Formula (20),

$$q_5 = atan2(wrist * R_w(2, 3),\quad wrist*R_w(1, 3)) \tag{23}$$

$$q_7 = atan2(wrist * R_w(3, 2),\quad -1 * wrist * R_w(3, 1)). \tag{24}$$

According to the above, given the end pose T_d and the elbow angle Ψ, we can obtain eight sets of discrete solutions. Then, given the three introduced control parameters, we can obtain the only analytical inverse solution.

When calculating $\Sigma_D^{\Psi=0}$ in Equation (6), if W is on the Z_0 axis, then the vectors X^Σ and Z_0 are parallel, and the product of the two results in a zero vector. This result cannot be used as Y^Σ, and this case is special. $\mathbf{Y}^\Sigma = \begin{bmatrix} 0 & 1 & 0 \end{bmatrix}^{\mathrm{T}}$ is directly taken. The *plSEW* plane is shown in Figure 8.
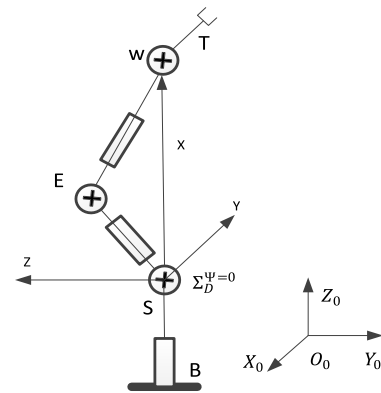

FIGURE 8. Analysis of the singularity of the inverse algorithm.

D. WORKSPACE

The above kinematics inverse solution is only the point mapping in the operation space to the joint space. The discrete mapping occurs between points, and the motion of the robot is continuous. The continuous path point in the operation space, which is mapped to the joint space, should produce the continuous joint angular sequence. This issue involves motion planning and is closely related to the workspace. From the kinematics inverse solution, a wrist W position that corresponds to the pose of the end effector always exists. The W position of the wrist reflects the position of the end effector. The two positions should be determined by the first four joint angles, and the three latter joint angles determine the posture of the end effector.

In the inverse kinematics solution, three control parameters (elbow, arm, and wrist) are introduced. The positive or negative parameter values will change the joint angle and yield two pairs of solutions. When mapping a continuous path in an operating space into a joint angle, the positive and negative values of the three control parameters cannot be arbitrarily changed. Otherwise, the joint angle will change suddenly, and the corresponding joint trajectory will no longer be continuous.

Table 2 lists the relationship between the two solutions. When $q_4 = 0$ or q_4 is close to 0, the positive and negative values of the elbow can be changed, and the obtained joint angle q_4 remains continuous. Notably, when q_4 is 0, the end

TABLE 2. Connection of discrete multiple solutions.

	First solution	Second solution
elbow	q_4	$-q_4$
arm	q_2, q_1, q_3	$-q_2, q_1 \mp pi, q_3 \mp pi$

effector is located near the working space boundary. q_2 is associated with q1 and q3. Thus, even in the neighborhood of $q_2 = 0$, the arm's positive and negative values cannot be changed. Otherwise, q_1 or q_3 may change, or the joint limit may be exceeded. The conclusion of the above derivation is that the working space must be divided according to the robot position configuration, as shown in Table 3.

TABLE 3. Division of the workspace.

Configuration space		Workspace block	Instructions
arm = +1	elbow = +1	Workspace block 1	Workspace blocks 1, 2 can communicate when the path contains the corresponding end position when q4 = 0.
arm = +1	elbow = −1	Workspace block 2	
arm = −1	elbow = +1	Workspace block 3	Workspace blocks 1, 2 can communicate when the path contains the corresponding end position when q4 = 0.
arm = −1	elbow = −1	Workspace block 4	

If the path of an operation space is not contained in the workspace corresponding to a configuration space block, mapping to the joint space will cause the joint angle to exceed the limit. Therefore, a principle of path planning is proposed here. That is, the planned path must be included in the workspace corresponding to a location configuration block. If the path can be connected in two workspace blocks, then the union of the two workspace blocks can be planned.

The point set of the position of the elbow E in the three-dimensional space is part of a spherical surface, which depends on the limit of the rotation angle of Joints 1 and 2. The distribution of elbow position E when the arm takes + 1, that is, $q_2 \in [0\ 2\pi/3]$, is shown in Figure 9. The distribution of elbow position E when the arm takes −1, that is, $q_2 \in [0\ -2\pi/3]$, is shown in Figure 10.
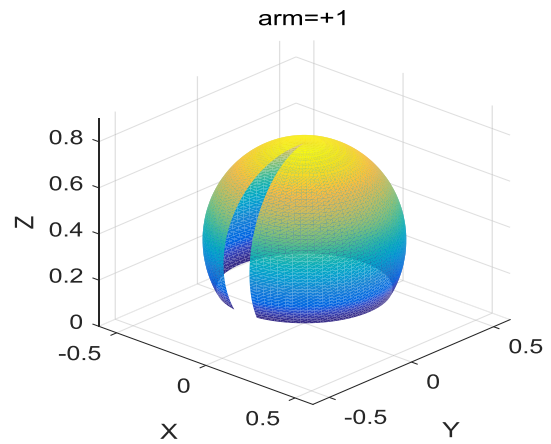

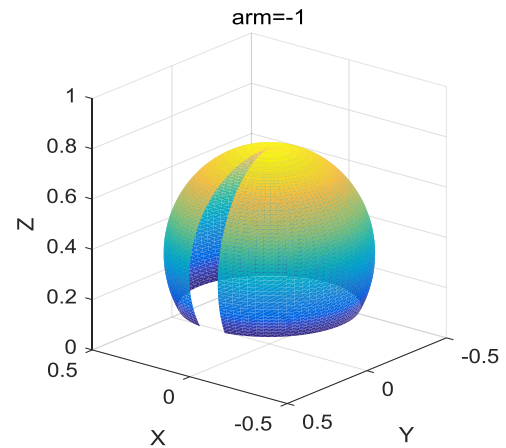**FIGURE 9.** Elbow joint position when arm = +1.

FIGURE 10. Elbow joint position when arm = −1.

When joint q_4 takes $\pm 2\pi/3$, W is closest to the shoulder joint position S. The distribution of W in the space, which is a closed but incomplete sphere, with the rotation of q_1, q_2 and q_3 is shown in Figures 9 and 10.

When joint q_4 is 0, W is farthest from the shoulder joint position S. At this moment, the distribution of W in space is still a closed but incomplete spherical surface. Figure 11 shows the W position distribution obtained using the Monte Carlo method, and Figure 12 presents the spherical part of the robot W position limit.

III. KINEMATIC INVERSE SOLUTION UNDER LIMIT JOINTS
For each end pose, by changing the elbow angle Ψ, a continuous joint vector can be obtained. If a solution satisfying the joint limit exists, then the elbow angle Ψ can be set to achieve the limit of the joint avoidance. From this condition, the joint limit rotation angle can be mapped to Ψ, and the Ψ range can be obtained to satisfy the limit of the seven joint angles.

$$\mathbf{Rot}(x, \Psi) = \begin{bmatrix} 1 & 0 & 0 \\ 0 & \cos\Psi & -sin\Psi \\ 0 & \sin\Psi & \cos\Psi \end{bmatrix} \quad (25)$$
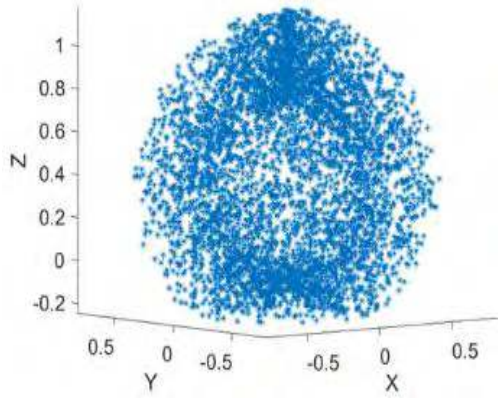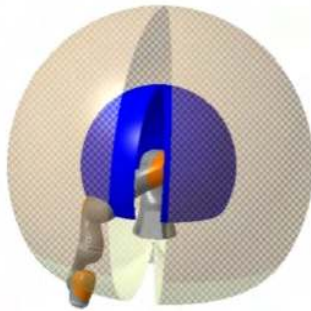
FIGURE 11. W location distribution.

FIGURE 12. Spherical part of W limiting position.

through the following proof:

$$\mathbf{Rot}\,(x, \Psi) = I_3 + \sin \Psi\,[x \times] + (1 - \cos \Psi)\,[x \times]^2. \quad (26)$$

In Formula (26), I_3 is the 3×3 unit matrix, and $[x \times]$ is an antisymmetric matrix consisting of unit vectors x.

This formula is expanded to obtain the transformation function for Ψ; bringing in Equation (10) can yield the Σ_D visual expression on Ψ. By bringing Σ_D into Equation (11), we can obtain

$$R_S = A_s \sin \Psi + B_s \cos \Psi + C_s. \quad (27)$$

In the above formula, $A_s = \Sigma_D^{\Psi=0} \times [x \times] \times \Sigma_o^T$; $A_s(i, j)$ is a_{sij}; $B_s = -1 \times \Sigma_D^{\Psi=0} \times [x \times]^2 \times \Sigma_o^T$; $B_s(i, j)$ is b_{sij}; $C_s = (x \times x^T) \times \Sigma_o^T$; $C_s(i, j)$ is c_{sij}.

From the spherical hinge transformation formula,

$$\mathbf{R}_s\,(q_1, q_2, q_3) = \begin{bmatrix} * & * & C_1 S_2 \\ * & * & S_1 S_2 \\ -C_3 S_2 & S_3 S_2 & C_2 \end{bmatrix} \quad (28)$$

From the correspondence between Formulas (27) and (28), we can obtain

$$\cos q_2 = a_{s33} \sin \Psi + b_{s33} \cos \Psi + c_{s33} \quad (29)$$

The range of $\cos q_2$ is deduced from the range of q_2, and the range of values of Ψ satisfying the limit of q_2 is further calculated. For the convenience of calculation, the software

MATLAB is adopted to solve the interval algorithm for the sine function inequality using Formula (30).

$$C \le A \sin \beta + B \cos \beta \le D \quad (30)$$

In this formula, $\beta \in \left[-\pi \ \pi \right]$ and A, B, C and D are arbitrary real numbers.

From the correspondence between Formulas (27) and (28), we can obtain

$$\tan q1 = \frac{S_1 S_2}{C_1 S_2} = \frac{a_{s23} \sin \Psi + b_{s23} \cos \Psi + c_{s23}}{a_{s13} \sin \Psi + b_{s13} \cos \Psi + c_{s13}} \quad (31)$$

Similar equations exist for q_3, q_5, q_7. Here, we use β to represent one of the angles; then, the problem is expressed as

$$\tan \beta = \frac{a_n \sin \Psi + b_n \cos \Psi + c_n}{a_d \sin \Psi + b_d \cos \Psi + c_d}. \quad (32)$$

In the formula, $\beta_1 \le \beta \le \beta_2$, and $\left[-pi/2 \ pi/2 \right] \subset \beta$.

We set up $f_n = a_n \sin \Psi + b_n \cos \Psi + c_n$, $f_d = a_d \sin \Psi + b_d \cos \Psi + c_d$. The range of $\tan \beta$ depends on the positive and negative values of $\cos \beta$, $\sin \beta$. The positive or negative values of $\sin \beta$, $\cos\beta$, and the positive or negative values of f_n, f_d depend on the values of the arm and wrist. See Table 4.

TABLE 4. Impact on tan β of the values of the arm and wrist.

Positive and negative classification		β takes q_1, q_3		β takes q_5, q_7	
		arm = +1	arm = −1	wrist = +1	wrist = −1
f_n	$\sin \beta$	same	reverse	same	reverse
f_d	$\cos \beta$	same	reverse	same	reverse

The following is for the case of arm = +1, wrist = +1, and the value of $\tan \beta$ within $\left[-\pi \ \pi \right]$, as shown in Figure 13.

Segment β separately solves the interval of Ψ. In $\left[-\frac{\pi}{2} \ \frac{\pi}{2} \right]$, one of the intervals of the Ψ satisfying the β requirements is $f_d > 0$. In $\left[-\pi \ -\frac{\pi}{2} \right]$, $f_d < 0$, $f_n < 0$, $f_n/f_d > \tan \beta_1$. In $\left[\pi/2 \ \pi \right]$, $f_d < 0$, $f_n > 0$, $f_n/f_d < \tan \beta_2$, $f_n/f_d > \tan \beta_1$ and $f_n/f_d < \tan \beta_2$ can also be solved as the sine inequality algorithm of Equation (30).

Overall, the interval of Ψ for satisfying $\beta_1 \le \beta \le \beta_2$ is

$$\{f_d > 0\} \cup \left\{ (f_d < 0) \cap (f_n < 0) \cap \left(f_n/f_d > \tan \beta_1 \right) \right\}$$
$$\cup \left\{ (f_d < 0) \cap (f_n > 0) \cap \left(f_n/f_d < \tan \beta_2 \right) \right\} \quad (33)$$

For the seven joints, by removing the fourth joint, the ψ interval of the joint-avoiding limit is

$$\Psi' = \Psi_1' \cap \Psi_2' \cap \Psi_3' \cap \Psi_5' \cap \Psi_6' \cap \Psi_7' \quad (34)$$

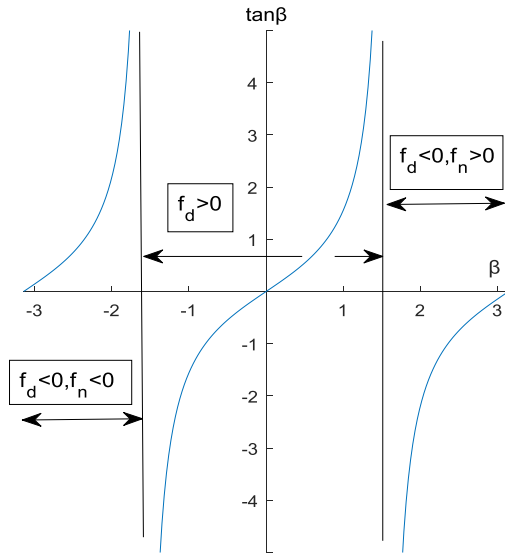In the formula, $\Psi'_i (i = 1, 2, 3, 5, 6, 7)$ is the interval of the joint q_i limit.

FIGURE 13. tan β value section division by plus or minus f_n, Cf_d.

IV. INVERSE SOLUTION UNDER THE CONSTRAINT OF OBSTACLE AVOIDANCE

Using the self-motion of the elbow joint in space, the elbow angle range where the robot avoids obstacles can be found. For a given end pose T_d, the position of the shoulder joint S and the wrist joint W in space is fixed and can be represented in the end pose according to the derivation in the first chapter. The key is using the elbow angle Ψ to indicate the position of the elbow in space. The pedal on the line SW via E is O_e, and $\left\| \vec{O_e E} \right\|$ can be determined and set to H. O_e is the origin of the coordinate system, $\vec{SW}$ is the positive direction of the X axis and $O_e E$ is the positive direction of the Z axis. The coordinate system $O_e - X_e Y_e Z_e$ is established as shown in Figure 14, and the solution formula is shown as (35).

$$\begin{cases} X_e = \vec{SW} / \left\| \vec{SW} \right\| \\ Y_e = (Z \times X_e) / \| Z \times X_e \| \\ Z_e = X_e \times Y_e \end{cases} \tag{35}$$

Vector $\vec{SO_e}$

$$\vec{SO_e} = \frac{\vec{SW}}{\left\| \vec{SW} \right\|} \left\| \vec{SE} \right\| \cos \angle ESW, \tag{36}$$
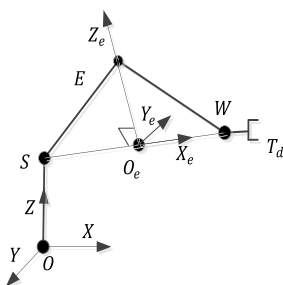

FIGURE 14. Coordinate system $O_e - X_e Y_e Z_e$.

Vector $\vec{OO_e}$

$$\vec{OO_e} = \vec{OS} + \vec{SO_e} \tag{37}$$

The homogeneous transformation matrix T_e of $O_e - X_e Y_e Z_e$ is known.

$$\mathbf{T}_e = \begin{bmatrix} X_e & Y_e & Z_e & \vec{OO_e} \\ 0 & 0 & 0 & 1 \end{bmatrix} \tag{38}$$
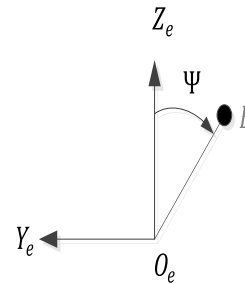

FIGURE 15. Point E in $O_e - X_e Y_e Z_e$.

Figure 15 illustrates the position of E in $O_e - X_e Y_e Z_e$. $\vec{O_e Z_e}$ is regarded as the starting line of the elbow angle Ψ, and the coordinate of E in $O_e - X_e Y_e Z_e$ is as in (39).

$$\begin{cases} E^{Z_e} = H \cos \Psi \\ E^{Y_e} = -H \sin \Psi \\ E^{X_e} = 0 \end{cases} \tag{39}$$

We can find the coordinate of E in $O - XYZ$.

$$\begin{bmatrix} E \\ 1 \end{bmatrix} = \mathbf{T}_e \begin{bmatrix} E^{X_e} \\ E^{Y_e} \\ E^{Z_e} \\ 1 \end{bmatrix} \tag{40}$$

S, E, W, and T are four known point positions, and the positions of the connecting rod SE, connecting rod EW and connecting rod WT are determined by the end effector pose and elbow angle extraction values. The collision detection algorithm can be utilized to test whether the three links of the robot collide with the obstacle model.

WT does not change with the elbow angle because the former is related only to the end pose. If WT collides, then only the end pose can be adjusted. If WT does not collide, then Ψ is discretized in $[-pi, pi]$. For each sample point, whether the links SE and EW intersect with the obstacle is tested, as shown in Figure 16. When the discretization is adequately small, the collision occurrence Ψ interval is a continuous interval. According to whether each sample point collides or not, a Ψ range in which collision does not occur may be obtained, that is an obstacle avoidance elbow angle range, which may be a union of several cells. Collision detection is represented by the functionisCollision(φ), which returns TRUE if a collision occurs and FALSE otherwise. The input parameter φ represents a discrete point value of
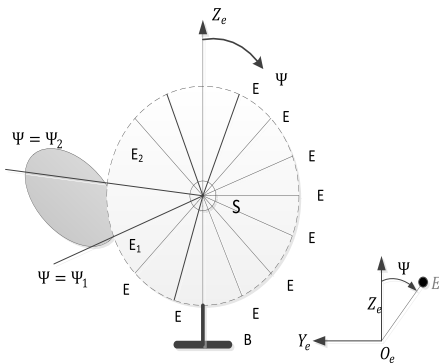
FIGURE 16. Obstacle avoidance arm angle section and obstacle.

the elbow angle. The result is stored in the linked list data structure Ψ.

Figure 17 illustrates the algorithm flowchart. Ψ obtained by the algorithm is a linked list with a total of even number values; the odd-numbered values and the next-to-adjacent value form an obstacle avoidance arm angle interval. Two or more subintervals may exist in the linked list, and the union of intervals includes all elbow angles that can avoid obstacles. This interval value is taken into the kinematic inverse solution formula to obtain a joint-free rotation vector of the robot arm.

V. ALGORITHM VERIFICATION AND SIMULATION

In this research, the MATLAB Robotics Toolbox is utilized to establish the robot model, and an algorithm program for inverse kinematics, joint avoidance limit, and elbow angle range is written to verify the effectiveness of the proposed method. Using the Link and SerialLink classes in the toolbox, the robot model is established as shown in Figure 18, which depicts the pose when the joint rotation angle is 0.

A. KINEMATIC INVERSE SIMULATION

Setting the end trajectory to an ellipse, the equation for the ellipse is shown in Equation (52).

$$\begin{cases} x = 0.3 \\ y = 0.2 + 0.2 \cos\alpha \\ z = 0.4 + 0.2 \sin\alpha \end{cases} \tag{41}$$

In the formula, $-pi \leq \alpha \leq pi$.

The end posture is set to a posture that rotates approximately 60 degrees around its X axis. In MATLAB, α is discretized to obtain the α sequence and then simulated. Setting the elbow angle Ψ to 0 and elbow = +1, Figure 19 presents the simulation.

Apparently, when the elbow = +1, the plane plSEW is vertical, and the elbow position is directly above the SW line, which is consistent with the above analytical solution process. In addition, the end trajectory is a complete and accurate ellipse, the starting point and the ending point are closed, the end pose does conform to the setting and the analysis inverse solution has no principle error or joint rotation angle drift. Therefore, the kinematics analysis is correct.
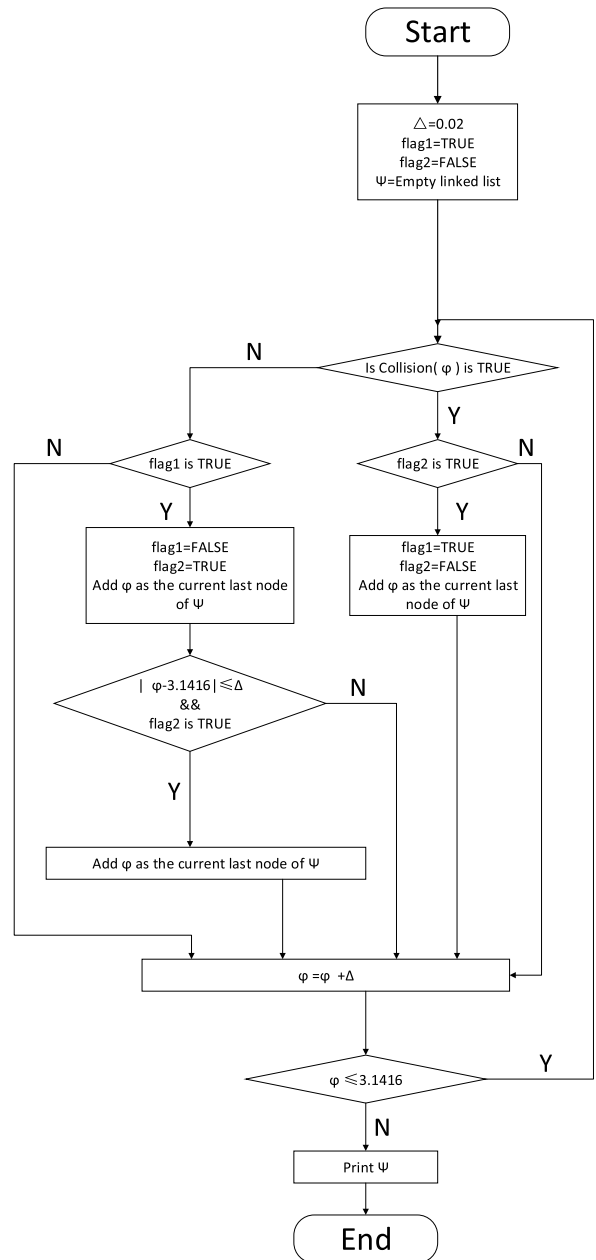

FIGURE 17. Solution flowchart of obstacle avoidance arm angle.

Figure 20 presents the joint angle change obtained by setting the arm = +1 and wrist = +1:

from the figure, joint q7 exceeds the joint limit and a mutation occurs at $\pm 180°$. When setting the wrist = −1, the inverse solution derivation process shows that q5, q7 increase by π and modulo 2π, and q6 becomes the opposite number.

Figure 21 presents the results for setting arm = +1, wrist = −1. q7 is completely within the limit in this setting and avoids joint overrun because the arm does not change the setting. Therefore, q1, q2, and q3 do not change. Similar to this joint rotation beyond the $\pm 180°$ and mutation, only by setting these three parameters can we avoid joint overrun.
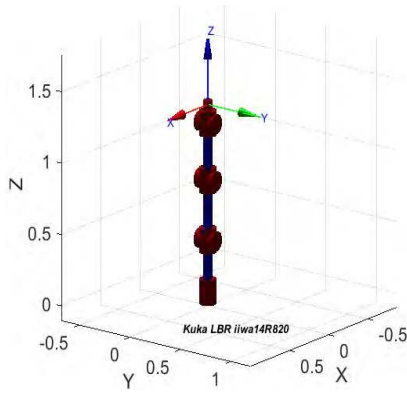
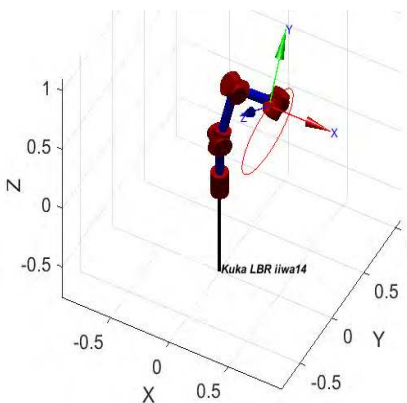**FIGURE 18.** Model of robot (joint angles are all 0°).

FIGURE 21. Change in joint angle.

FIGURE 19. Robot terminal trajectory simulation.
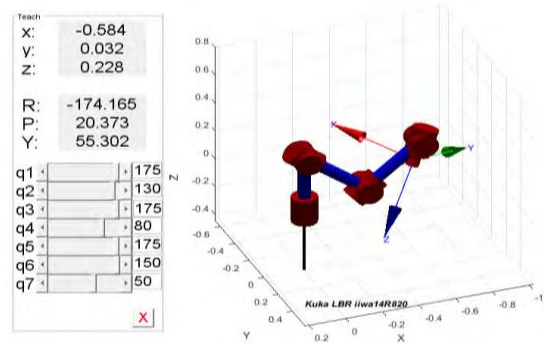
FIGURE 22. Robot simulation interface.

joint variables exceeding the joint limit is set.

$$\mathbf{q} = \begin{bmatrix} 175° & 130° & 175° & 80° & 175° & 150° & 50° \end{bmatrix} \quad (42)$$

Amongst them, q1, q2, q3, q5 and q6 all exceed the limit. Even if the value of arm or wrist is changed, the joint limit is still exceeded.

The end position $\mathbf{p}_e= [−0.584, 0.032, 0.228]$ and the attitude RPY angle $\phi_e = [−174.165°, 20.373°, 55.302°]$ are obtained and converted to an end-transform homogeneous transformation matrix $\mathbf{T}_d$.

$$\mathbf{T}_d = \begin{bmatrix} 0.5336 & −0.7707 & 0.3481 & −0.5840 \\ −0.8381 & −0.5372 & 0.0953 & 0.0320 \\ 0.1136 & −0.3426 & −0.9326 & 0.2280 \\ 0 & 0 & 0 & 1 \end{bmatrix}$$
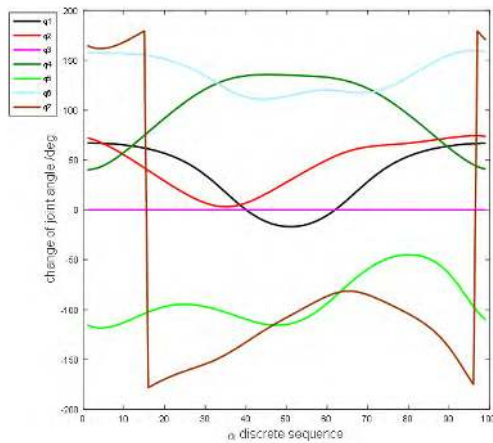
$$(43)$$

FIGURE 20. Change in joint angle.

For a situation exceeding the joint limit but not mutating at the ±180°, the elbow angle can be set to prevent joint overrun.

B. AVOIDANCE JOINT LIMIT ELBOW ANGLE INTERVAL SIMULATION

In MATLAB, the SerialLink.teach () function is used to bring up the simulation interface. As shown in Figure 22, a set of

The range of elbow angle Ψ is $[−pi, pi]$. This interval is distinguished, and arm = +1, elbow = +1, wrist = +1 are set to obtain the joint space vector corresponding to Ψ. For each discrete Ψ value, the seven joint rotation angles are calculated. Figure 23 presents the joint rotation angles q2, q4 and q6. The data cursor function is utilised to capture the Y axis limit value. Then, the corresponding elbow angle value is obtained, as shown in Figure 24.
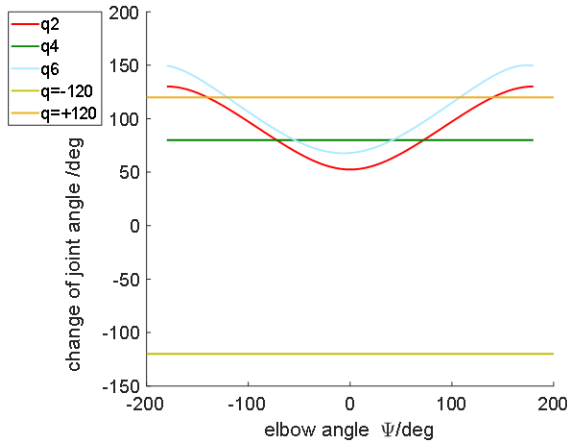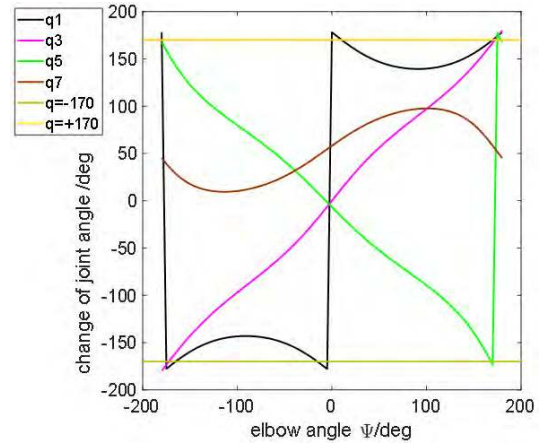
FIGURE 23. Changes in q2, q4 and q6 joint angles.
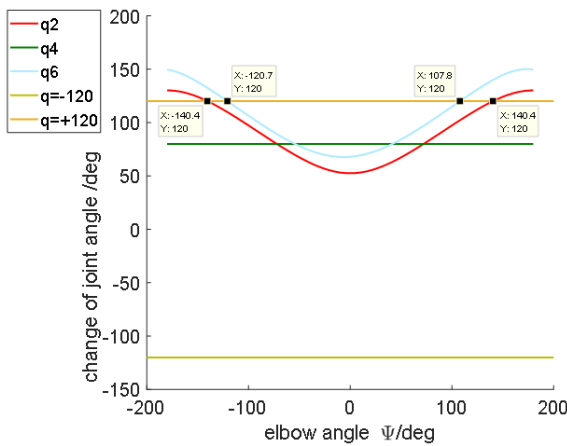

FIGURE 25. Changes in q1, q3, q5 and q7 joint angles.
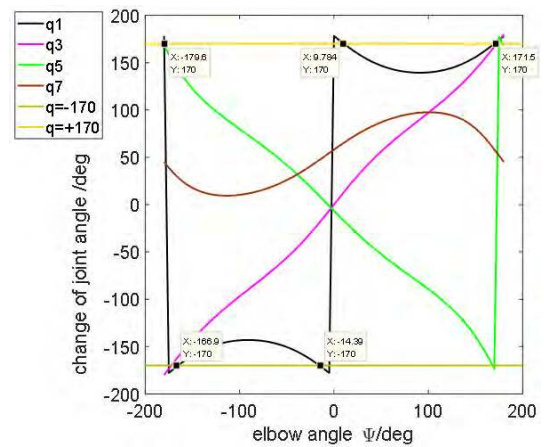

FIGURE 24. Changes in q2, q4 and q6 joint angles.

FIGURE 26. Changes in q1, q3, q5 and q7 joint angles.

TABLE 5. Joint limit avoidance arm angle sections.

Ψ'_i	Limit interval of avoidance joint
Ψ'_2	[-2.4483, 2.4483]
Ψ'_6	[-2.1080, 1.8828]

TABLE 6. Joint limit avoidance arm angle sections.

Ψ'_i	Limit interval of avoidance joint
Ψ'_1	$[-2.8833, -0.2680] \cup [0.1828 \quad 2.9654]$
Ψ'_3	$[-3.0076 \quad 3.0076]$
Ψ'_5	$[-3.1416 \quad 2.9363] \cup [3.1216 \quad 3.1416]$
Ψ'_7	$[-3.1416, 3.1416]$

Note that π is taken as 3.1416 in MATLAB.

The limit of the Ψ arc system obtained by the program is shown in Table 5. By comparing the results, we can see that the results of the algorithm are consistent with the results obtained in the graph.

Figure 25 presents the change curves of joint angles q1, q3, q5, and q7. According to the limit value of the Y-axis of the q1 curve, we can determine that the elbow angle is obtained as shown in Figure 26. We calculate the limit range of the Ψ arc system, as shown in Table 6.

The results of the algorithm are consistent with the findings obtained in the graph. We take the intersection to obtain the elbow angle range whilst avoiding the seven joint rotation angles exceeding the limit.

$$\Psi' = \begin{bmatrix} -2.1080 & -0.2680 \end{bmatrix} \cup \begin{bmatrix} 0.1828 & 1.8828 \end{bmatrix} \quad (44)$$

For each end effector pose, after setting the value of the arm, elbow, and wrist, the algorithm can be used to calculate the range of the avoiding limit of each angle; then, the intersection can be utilized to determine the elbow angle interval that satisfies the limit of each joint angle.

C. OBSTACLE AVOIDANCE SIMULATION

An obstacle environment model is established by using a cuboid and a cylinder, and the desired position of the end of the manipulator is set. As shown in Figure 27, the obstacle avoidance elbow angle range obtained is $\begin{bmatrix} 1.5584 & 2.1784 \end{bmatrix}$.
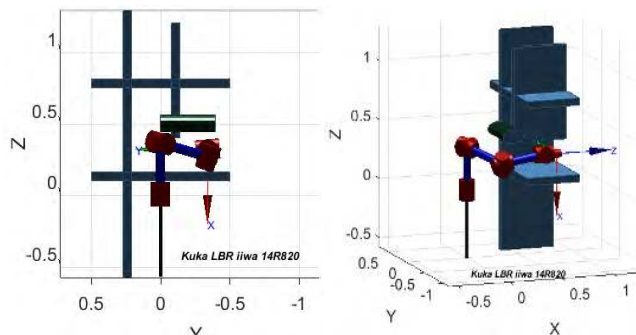
FIGURE 27. Robot obstacle environmental model.
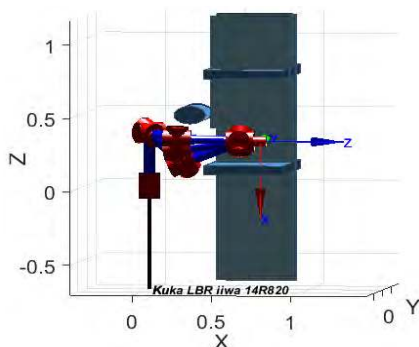
FIGURE 28. Manipulator inverse kinematics obstacle avoidance configuration set.

FIGURE 29. Conventional trajectory planning method paths 1 and 2.
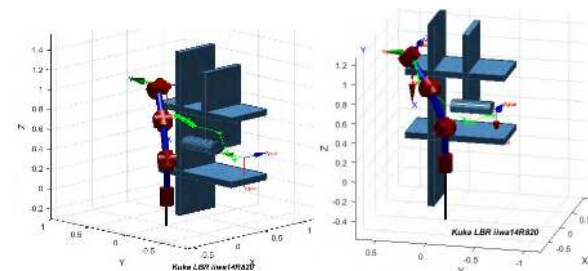
FIGURE 30. Proposed trajectory planning method paths 1 and 2.

Figure 28 presents the motion of the manipulator on the elbow angle range. At the limit position of the manipulator, the manipulator is on the point of collision with the obstacle. This method is fully proven to solve nearly all the inverse kinematic solutions of obstacle avoidance.

VI. COMPARATIVE TEST

The redundant manipulator performs a grabbing task in an unstructured environment. At present, it is generally adopted to capture the target space position, solve the joint angles and then repeatedly adjust the self-motion freedom, avoid obstacles and avoid joint motion overrun. The trajectory planning method must be repeatedly solved and judged multiple times before the task can be completed; the efficiency is low, and the planning difficulty is high.

In the application of the proposed method, the elbow angle is selected as the supplementary control parameter, which can make the joint angle of each solution satisfy the obstacle and joint overrun, this allows an explicit solution to the inverse solution of the redundant DOF robot. Thus, the efficiency of trajectory planning is significantly improved. In the workspace between the redundant degree of freedom robot arm and the grab target object, obstacles in the X and Y directions are set. Figure 29 shows the path generated by the robotic arm in the obstacle environment using a conventional trajectory planning method. Paths 1 and 2 show the results of the 248th and 363rd adjustment operations, respectively. Apparently, the planned paths are different, the number of
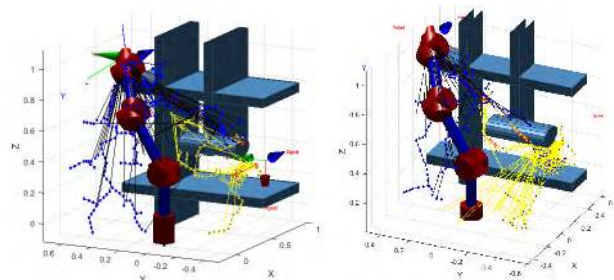
adjustments is large and many path-jump points exist. In the same workspace, the redundant robotic arm (Figure 30) tests the path generated by the proposed algorithm in an obstacle environment. Paths 3 and 4 show the results of the 25th and 16th adjustments, respectively. Apparently, the number of adjustments of the two planning paths is significantly reduced. It has a certain smoothness and is in line with the natural movement of the human arm.

VII. CONCLUSION

(1) The self-motion characteristics of the 7R human redundant manipulator are described by the elbow angle parameter. A kinematics inverse solution model of the manipulator with the elbow angle as the seventh constraint is established.

(2) On the basis of the multiplicity of inverse solutions, the manipulator workspace is divided; for the continuous end-path, a method of selecting the inverse solution from the discrete multiple solutions is given, which can obtain the continuous joint angle vector without Mutation.

(3) Taking the elbow angle as the parameter, the mapping relationship between the elbow and joint angles is established to solve the elbow angle interval satisfying the joint limit. Then, all the inverse solutions of the joint limit can be obtained by this interval.

(4) The mapping relationship between the elbow angle and the elbow joint is established, and the pose of each connecting rod of the manipulator is obtained. The elbow angle is discretized, and the collision detection algorithm is adopted to test all the values of the elbow angle. On the basis of whether the arm collides with an obstacle, the elbow angle interval of the collision avoidance is obtained. This interval

can be utilized to obtain the inverse solution of all obstacle avoidances in the given end pose.

REFERENCES

[1] D. Zhou, L. Ji, Q. Zhang, and X. Wei, "Practical analytical inverse kinematic approach for 7-DOF space manipulators with joint and attitude limits," *Intell. Service Robot.*, vol. 8, no. 4, pp. 215–224, 2015.

[2] L. Sciavicco and B. Siciliano, "A solution algorithm to the inverse kinematic problem for redundant manipulators," *IEEE J. Robot. Autom.*, vol. RA-4, no. 4, pp. 403–410, Aug. 1988.

[3] W. Liu, D. Chen, and J. J. Steil, "Analytical inverse kinematics solver for anthropomorphic 7-DOF redundant manipulators with human-like configuration constraints," *J. Intell. Robot. Syst.*, vol. 86, no. 1, pp. 63–79, 2017.

[4] I. Kuhlemann, A. Schweikard, F. Ernst, and P. Jauer, "Robust inverse kinematics by configuration control for redundant manipulators with seven DOF," in *Proc. Int. Conf. Control, Autom. Robot.*, 2016, pp. 49–55.

[5] T. Nammoto and K. Kosuge, "An analytical solution for a redundant manipulator with seven degrees of freedom," *Int. J. Autom. Smart Technol.*, vol. 2, no. 4, pp. 339–346, 2012.

[6] H. H. An, W. I. Clement, and B. Reed, "Analytical inverse kinematic solution with self-motion constraint for the 7-DOF restore robot arm," in *Proc. IEEE/ASME Int. Conf. Adv. Intell. Mechatronics*, Jul. 2014, pp. 1325–1330.

[7] Z. Cui, H. Pan, Y. Peng, Z. Han, and D. Qian, "A novel inverse kinematics solution for a 7-DOF humanoid manipulator," in *Proc. IEEE Int. Conf. Mechatronics Automat.*, Aug. 2012, pp. 2230–2234.

[8] J. Zhang, W.-F. Xu, and D.-S. Meng, "Inverse kinematics resolution method of redundant space manipulator based on arm angle parameterization," in *Proc. IEEE Control Conf.*, Jul. 2013, pp. 6022–6027.

[9] H. Seraji, M. K. Long, and T. S. Lee, "Motion control of 7-DOF arms: The configuration control approach," *IEEE Trans. Robot. Autom.*, vol. 9, no. 2, pp. 125–139, Apr. 1993.

[10] A. Atawnih, D. Papageorgiou, and Z. Doulgeri, "Kinematic control of redundant robots with guaranteed joint limit avoidance," *Robot. Auto. Syst.*, vol. 79, pp. 122–131, May 2016.

[11] X. Huo, Y. Liu, H. Liu, and L. Jiang, "Inverse kinematic optimizations of 7R humanoid arms based on a joint parameterization," in *Proc. IEEE Int. Conf. Mechatronics Automat.*, Aug. 2014, pp. 113–118.

[12] M. Benzaoui, H. Chekireb, M. Tadjine, and A. Boulkroune, "Trajectory tracking with obstacle avoidance of redundant manipulator based on fuzzy inference systems," *Neurocomputing*, vol. 196, pp. 23–30, Jul. 2016.

[13] Y. Zhang and Z. Zhang, *Repetitive Motion Planning and Control of Redundant Robot Manipulators*. Beijing, China: Springer, 2014.

[14] L. Yan, Z. Mu, and W. Xu, "Analytical inverse kinematics of a class of redundant manipulator based on dual arm-angle parameterization," in *Proc. IEEE Int. Conf. Syst., Man Cybern.*, Oct. 2014, pp. 3744–3749.

[15] M. Shimizu, H. Kakuya, W. K. Yoon, K. Kitagaki, and K. Kosuge, "Analytical inverse kinematic computation for 7-DOF redundant manipulators with joint limits and its application to redundancy resolution," *IEEE Trans. Robot.*, vol. 24, no. 5, pp. 1131–1142, Oct. 2008.

[16] B. Siciliano *et al.*, *Robotics: Modelling, Planning and Control*. Springer, 2010.

[17] J. Oh, H. Bae, and J.-H. Oh, "Analytic inverse kinematics considering the joint constraints and self-collision for redundant 7DOF manipulator," in *Proc. IEEE Int. Conf. Robot. Comput.*, Apr. 2017, pp. 123–128.

[18] H. Moradi and S. Lee, "Joint limit analysis and elbow movement minimization for redundant manipulators using closed form method," in *Proc. Int. Conf. Intell. Comput. (ICIC)*, Hefei, China, 2005, pp. 423–432.

[19] C. Ericson, *Real-Time Collision Detection*. Boca Raton, FL, USA: CRC Press, 2004.

[20] H. Shen, H. Wu, Y. Jiang, C. Yan, and B. Chen, "Obstacle avoidance algorithm for 7-DOF redundant anthropomorphic arm," *J. Control Sci. Eng.*, vol. 2015, Dec. 2015, Art. no. 540259.

[21] G. Xiao-Qing *et al.*, "Multiple mobile-obstacle avoidance algorithm for redundant manipulator," *J. Beijing Inst. Technol.*, vol. 25, no. 1, pp. 71–76, 2016.

[22] X.-P. Hu, K. Xie, and F.-Y. Zuo, "(Hunan provincial key laboratory of health maintenance for mechanical equipment, Hunan University of Science and Technology, Xiangtan 411201,China);obstacle avoidance path planning for manipulator based on improved artificial potential field," *Meas., Control Technol.*, 2012.

[23] H. Toshani and M. Farrokhi, "Real-time inverse kinematics of redundant manipulators using neural networks and quadratic programming: A Lyapunov-based approach," *Robot. Auton. Syst.*, vol. 62, no. 6, pp. 766–781, 2014.

[24] H. Toshani and M. Farrokhi, "Kinematic control of a seven DOF robot manipulator with joint limits and obstacle avoidance using neural networks," in *Proc. IEEE Int. Conf. Control, Instrum. Automat.*, Dec. 2012, pp. 976–981.

[25] Y. Zhang and J. Wang, "Obstacle avoidance for kinematically redundant manipulators using a dual neural network," *IEEE Trans. Syst. Man, Cybern. B, Cybern.*, vol. 34, no. 1, pp. 752–759, Feb. 2004.

[26] M. H. Korayem and A. Nikoobin, "Maximum payload path planning for redundant manipulator using indirect solution of optimal control problem," *Int. J. Adv. Manuf. Technol.*, vol. 44, no. 7, pp. 725–736, 2009.

[27] M. H. Korayem, M. Irani, and S. R. Nekoo, "Load maximization of flexible joint mechanical manipulator using nonlinear optimal controller," *Acta Astronautica*, vol. 69, nos. 7–8, pp. 458–469, 2011.

[28] C.-Y. E. Wang, W. K. Timoszyk, and J. E. Bobrow, "Payload maximization for open chained manipulators: Finding weightlifting motions for a Puma 762 robot," *IEEE Trans. Robot. Autom.*, vol. 17, no. 2, pp. 218–224, Apr. 2001.

[29] M. H. Korayem, R. A. Esfeden, and S. R. Nekoo, "Path planning algorithm in wheeled mobile manipulators based on motion of arms," *J. Mech. Sci. Technol.*, vol. 29, no. 4, pp. 1753–1763, 2015.

[30] M. H. Korayem, V. Azimi, H. Vatanjou, and A. H. Korayem, "Maximum load determination of nonholonomic mobile manipulator using hierarchical optimal control," *Robotica*, vol. 30, no. 1, pp. 53–65, 2012.

MINGDE GONG received the Ph.D. degree from Jilin University, China, in 2003. He is currently a Professor and Ph.D. Supervisor with the School of Mechanical Engineering, Yanshan University, China. His main research interests include teleoperation robot technology, and transmission and control of construction machinery.

XIANGDONG LI received the M.A. degree in mechatronics from Jilin University, China, in 2017. He is currently an Engineer with SINOMACH Intelligence Technology Co., Ltd., Guangzhou, China.

LEI ZHANG is currently pursuing the M.A. degree with the School of Mechanical Science and Engineering, Jilin University, China.

• • •